

Sustainable Food Technology

Accepted Manuscript

This article can be cited before page numbers have been issued, to do this please use: S. Udompaisarn, P. Chotiphantawanon, S. Kuhaudomlarp, R. Srikuea, S. Wangwongpaiboon, W. Watcharanapapan, T. Soonkum, D. Laohasinnarong, U. Suriya and T. Janvilisri, *Sustainable Food Technol.*, 2025, DOI: 10.1039/D5FB00756A.



This is an Accepted Manuscript, which has been through the Royal Society of Chemistry peer review process and has been accepted for publication.

Accepted Manuscripts are published online shortly after acceptance, before technical editing, formatting and proof reading. Using this free service, authors can make their results available to the community, in citable form, before we publish the edited article. We will replace this Accepted Manuscript with the edited and formatted Advance Article as soon as it is available.

You can find more information about Accepted Manuscripts in the [Information for Authors](#).

Please note that technical editing may introduce minor changes to the text and/or graphics, which may alter content. The journal's standard [Terms & Conditions](#) and the [Ethical guidelines](#) still apply. In no event shall the Royal Society of Chemistry be held responsible for any errors or omissions in this Accepted Manuscript or any consequences arising from the use of any information it contains.

Sustainability Spotlight Statement

Cellular agriculture offers a path to sustainable protein production, but its scalability is hindered by the high cost of media components needed for muscle cell differentiation. We address this major bottleneck by pioneering a multi-criteria chemical screening to identify **methylergometrine**, an affordable, clinically-approved compound, as a potent driver for transforming muscle stem cells into mature muscle fibers. This compound drastically reduces the reliance on expensive growth factors, cutting production costs for cultured meat. Our discovery, including a dual-phase chemical strategy to accelerate tissue formation, provides a chemically-defined, cost-effective method to achieve industrial-scale cultivated protein. This work directly supports UN **SDG 2 (Zero Hunger)** by making sustainable protein accessible and **UN SDG 12 (Responsible Consumption and Production)** by offering an efficient, resource-light alternative to conventional meat farming.



1 Targeted modulation of FGFR1 enhances myogenic 2 differentiation for cultured meat production

3 *Somsiri Udompaisarn^a, Prant Chotiphantawanon^b, Sakonwan Kuhaudomlarp^b, Ratchakrit*
4 *Srikuea^c, Sittiwat Wangwongpaiboon^c, Wasina Watcharanapapan^c, Thananya Soonkum^d, Dusit*
5 *Laohasinnarong^e, Utid Suriya^{b,*}, Tavan Janvilisri^{a,*}*

6 ^aDepartment of Microbiology, Faculty of Science, Chulalongkorn University, Bangkok, Thailand

7 ^bDepartment of Biochemistry, Faculty of Science, Mahidol University, Bangkok, Thailand

8 ^cDepartment of Physiology, Faculty of Science, Mahidol University, Bangkok, Thailand

9 ^dMahidol University-Frontier Research Facility, Mahidol University, Nakhon Pathom, Thailand

10 ^eDepartment of Clinical Sciences and Public Health, Faculty of Veterinary Science, Mahidol
11 University, Nakhon Pathom, Thailand

12 * Corresponding authors

13 T Janvilisri, Department of Microbiology, Faculty of Science, Chulalongkorn University,
14 Thailand E-mail: tavan.j@chula.ac.th

15 U Suriya, Department of Biochemistry, Faculty of Science, Mahidol University, Thailand E-mail:
16 utid.sur@mahidol.ac.th

17 **KEYWORDS:** molecular docking, FGFR1, cultured meat, myogenic differentiation, muscle
18 stem cells

19



20

21 **ABSTRACT**

22 The development of cultured meat offers a sustainable and ethical alternative to conventional
23 protein sources, yet its commercial scalability is hindered by the inefficient induction of terminal
24 myogenesis. Porcine muscle stem cells (PMSCs) are a promising cell source, but their effective
25 differentiation into mature muscle fibers remains a significant challenge. The fibroblast growth
26 factor receptor 1 (FGFR1) plays a pivotal role in maintaining the proliferative state of these cells,
27 making its inhibition a compelling strategy to promote differentiation. In this study, we employed
28 a multi-faceted approach, combining *in silico* and *in vitro* methods, to identify and validate novel
29 small-molecule FGFR1 modulators. A rigorous virtual screening of 872 compounds against the
30 FGFR1 tyrosine kinase domain, with subsequent filtering against the off-target p38 α MAPK,
31 identified methylethylergometrine as a highly promising candidate alongside the known
32 inhibitor dovitinib. Molecular dynamics simulations confirmed that both compounds form stable
33 complexes with FGFR1, a finding corroborated by saturation transfer difference-nuclear magnetic
34 resonance, which provided direct evidence of their distinct but complementary binding modes.
35 Subsequent *in vitro* functional assays in C2C12 mouse myogenic cells demonstrated that both
36 compounds enhance myogenic differentiation. Specifically, treatment with dovitinib and
37 methylethylergometrine led to a robust, dose- and phase-dependent upregulation of key myogenic
38 markers, including myosin heavy chain and myogenin. These findings confirm that dovitinib and



39 methylergometrine effectively promote myotube formation. Similar trends were also observed in
40 PMSCs. Our study introduces a novel strategy for stimulating terminal myogenesis through
41 targeted FGFR1 modulation, with significant implications for improving the efficiency and yield
42 of cell-based cultured meat production.

43 1. INTRODUCTION

44 Dietary protein is a critical nutrient for human growth, development, and healthy aging,
45 supporting physical development during early life and the maintenance of muscle mass, metabolic
46 health, and overall quality of life during aging [1, 2]. The escalating global demand for sustainable
47 and ethically sourced protein has propelled significant advancements in the development
48 of cultured meat [3, 4]. Among the diverse cell sources investigated, muscle stem cells, also known
49 as satellite cells, present a compelling platform due to their intrinsic capacity for robust
50 proliferation and efficient differentiation into mature muscle fibers [5, 6]. However, the
51 commercial scalability of cultured meat production remains hindered by several key challenges
52 including low cell yields, a decline in differentiation efficiency over successive cell passages, and
53 the prevalent use of animal-derived components in current culture media [7]. Addressing these
54 challenges necessitates a refined understanding of the molecular mechanisms governing
55 myogenesis, particularly the intricate balance between cell proliferation and terminal
56 differentiation.

57 Myogenic differentiation and myotube formation are widely recognized as fundamental
58 biological processes underlying muscle formation and are critical for the development of muscle-



59 like tissue in cultured meat systems. While large-scale cell expansion is required to generate
60 sufficient biomass, the efficiency of terminal differentiation ultimately defines product quality
61 such as muscle structure, protein composition, and meat texture. Without the transition from
62 mononuclear myoblasts to multinucleated myotubes, the final product lacks the structural integrity
63 of conventional muscle tissue (meat) [8, 9]. Therefore, inefficient differentiation leads to immature
64 and heterogeneous tissue structure and resulting in reducing product consistency, yield, scalability
65 and limiting the feasibility of sustainable cultured meat production. Currently, achieving efficient
66 and consistent myogenic differentiation remains challenging, even when sufficient cell biomass is
67 obtained [10]. Consequently, ensuring proper induction and control of myogenic differentiation is
68 essential for the development of scalable and reliable production systems for cultured meat.

69 Fibroblast growth factor receptor 1 (FGFR1) is a crucial regulator of muscle stem cell fate, acting
70 as a molecular switch that maintains a proliferative, undifferentiated state. Activation of FGFR1
71 signaling pathway promotes cell cycle progression by inhibiting key cyclin-dependent kinase
72 inhibitors like p21^{Waf1} and p27^{Kip1}, thereby favoring proliferation over differentiation [11].
73 Conversely, inhibiting or downregulating FGFR1 activity consistently promotes myogenic
74 differentiation. For example, the non-coding RNAs miR-133 and lncR-133a have been shown to
75 facilitate differentiation of C2C12 and goat muscle stem cells by downregulating FGFR1 and
76 attenuating ERK1/2 signaling [12, 13]. Similarly, leucine-rich repeats and transmembrane
77 domains 1 (LRTM1) negatively regulates FGFR1 by interfering with adaptor protein recruitment,
78 which reduces downstream ERK activation and enhances myotube formation [14]. These findings
79 collectively highlight FGFR1 inhibition as a highly promising therapeutic and biotechnological
80 strategy to trigger terminal myogenesis. However, approaches based on non-coding RNA



81 modulation or genetic manipulation of regulatory proteins are difficult to translate into practical
82 culture supplements. To date, defined small-molecule inhibitors suitable for incorporation into
83 muscle cell culture media remain limited. Therefore, in this study, the primary objective of this
84 study was to identify and validate novel pharmacological modulators of FGFR1 that accelerate the
85 transition of muscle stem cells from a proliferative state to terminal myogenesis, thereby
86 optimizing the structural and biochemical maturation of porcine-derived cultured muscle.

87 To identify novel compounds capable of modulating FGFR1, we employed an *in*
88 *silico* approach, leveraging molecular docking and molecular dynamics (MD) simulations to
89 assess the binding affinities and molecular interactions of potential candidates [15-17]. The
90 intracellular tyrosine kinase domain of FGFR1, a well-defined target known for its conserved two-
91 lobed kinase fold, was selected for these virtual screening efforts. To validate these *in silico*
92 predictions and confirm direct protein-compound interactions, we integrated nuclear magnetic
93 resonance (NMR) spectroscopy into our workflow [18]. Specifically, saturation transfer difference
94 (STD) NMR was used as a sensitive and powerful tool to rapidly detect ligand binding and map
95 the binding epitope, providing compelling experimental evidence of molecular interaction without
96 the need for protein immobilization or complex labeling [19].

97 In this study, we focused on two small-molecule compounds with the potential to modulate
98 FGFR1 signaling and influence myogenic differentiation. Dovitinib is a well-characterized multi-
99 kinase inhibitor with established anti-proliferative activity in various cancers through its inhibition
100 of FGFR1 signaling [20]. While its direct effects on skeletal muscle differentiation have not been



101 previously described, dovitinib's known ability to inhibit FGFR1 and enhance osteoblast
102 differentiation in other cell types suggests its potential to modulate myogenesis [21]. In parallel,
103 we investigated methylergometrine, an ergot alkaloid widely used in obstetrics for its uterotonic
104 properties [22]. Our preliminary data indicated that methylergometrine also interacts with tyrosine
105 kinases, positioning it as another intriguing candidate for inducing myogenic differentiation. By
106 evaluating both a well-established FGFR1 inhibitor (dovitinib) and a compound with novel,
107 unexplored kinase-binding properties (methylergometrine), we aimed to systematically assess
108 their potential to induce the differentiation of porcine muscle stem cells (PMSCs) and to explore
109 FGFR1 inhibition as a translatable strategy for cultured meat production.

110

111

112 2. MATERIALS AND METHODS

113 **2.1 Molecular docking and virtual screening.** To identify compounds with potential affinity for
114 FGFR1, we performed a comprehensive docking-based virtual screening process. The three-
115 dimensional crystal structures of the human FGFR1 tyrosine kinase domain in complex with the
116 inhibitor AZD4547 and the p38 α mitogen-activated protein kinase (p38 α MAPK) were retrieved
117 from the RCSB Protein Data Bank (PDB IDs: 4V05 [23] and 3ZSH [24], respectively). These
118 structures served as our protein targets for *in silico* analysis. A diverse compound library was
119 curated from two primary sources: a commercial nuclear receptor compound library from
120 MedChemExpress and a collection of 20 proprietary in-house compounds, including asiatic acid,



121 ticagrelor, and various alkaloid-like derivatives. All selected ligand structures were geometrically
122 optimized, and their protonation states were meticulously predicted at a physiological pH of 7.4
123 using the Open Babel software [25]. This rigorous preparation ensured the accuracy of subsequent
124 docking simulations. A total of 872 optimized compounds were prepared for virtual screening. The
125 binding site for docking was precisely defined by the coordinates of the co-crystallized ligands
126 within the FGFR1 and p38 α MAPK structures. A consistent grid box of 20 Å x 20 Å x 20 Å was
127 centered on these coordinates to encompass the entire active site. The virtual screening was
128 conducted using the AutoDock VinaXB software [26]. The simulations were executed on a Linux-
129 based computing system to handle the computational demands of screening such a large library.

130 **2.2 Molecular dynamics (MD) simulations.** To provide a more dynamic and biologically relevant
131 assessment of compound-protein interactions, we performed extensive all-atom MD simulations.
132 The initial complex structures for MD were generated from the top-scoring docking poses
133 identified in the virtual screening. Prior to simulation, the protonation states of ionizable amino
134 acids in the protein were assigned at physiological pH (pH = 7.4) using the PDB2PQR web server
135 [27]. The partial atomic charges of the ligand molecules were calculated using the General
136 AMBER Force Field version 2 (GAFF 2) within the Antechamber module of AMBER24. All
137 simulations were performed under periodic boundary conditions using the AMBER ff19SB force
138 field [28], which is optimized for biological macromolecules. The systems were solvated with the
139 explicit TIP3P water model and simulated under constant temperature (310 K) and pressure (1
140 atm) conditions (NPT ensemble). The entire system, including protein-ligand complex and solvent,



141 was gradually energy-minimized to relieve any steric clashes. Electrostatic interactions were
142 efficiently calculated using the particle mesh Ewald summation method [29], and the SHAKE
143 algorithm was applied to constrain all bonds involving hydrogen atoms, allowing for a larger
144 integration time step. Temperature was regulated using the Langevin thermostat, while pressure
145 was controlled by the Berendsen barostat [30-33]. Each production run was conducted for a
146 duration of 200 ns, with trajectories saved every 10 ps for post-dynamic analysis. The resulting
147 trajectories were analyzed using the CPPTRAJ module of AMBER to evaluate structural stability,
148 conformational changes, and key molecular interactions [34]. Finally, the binding free energy
149 (ΔG_{bind}) and decomposition ($\Delta G_{bind}^{residue}$) energy of the ligand-protein complex was estimated using
150 the Molecular Mechanics/Generalized Born Surface Area (MM/GBSA) method using the
151 MMPBSA.py module [35].

152 **2.3 Saturation transfer difference-nuclear magnetic resonance (STD-NMR) spectroscopy.** To
153 experimentally validate the direct binding of dovitinib and methylergometrine to FGFR1, we
154 utilized STD-NMR spectroscopy. Recombinant human FGFR1 protein was sourced from Abnova
155 (Cat. No. H00002260-G01). STD-NMR spectra were acquired on a Bruker Avance Ascend 600
156 MHz Spectrometer, equipped with a 5 mm BBO Prodigy CryoProbe. The probe temperature was
157 maintained at a constant 298 K. Samples were prepared in a 5 mm NMR tube containing 100 nM
158 of FGFR1 protein and a 15 mM concentration of either dovitinib or methylergometrine dissolved
159 in 600 μ L of deuterium oxide (D_2O). The residual peak (δ_H 4.79 ppm) was used as the internal
160 chemical shift reference. The spectrometer frequency was set to 600 MHz for both 1H and STD

161 dimensions. Spectral widths for the ^1H dimension was set at 9600 Hz with a 30° pulse angle. Each
162 acquisition involved a recycle delay of 2.5 s and 8 scans, collecting a total of 8 complex points for
163 the ^1H dimension.

164 **2.4 Cell culture and reagents.** The mouse myogenic cell line C2C12 (ATCC, CRL-1772) was
165 utilized as an *in vitro* model system. Cells were maintained in growth medium (GM) composed of
166 Dulbecco's modified Eagle's medium (DMEM; Gibco, 12800-017) supplemented with 10% (v/v)
167 fetal bovine serum (FBS; Gibco, A5256701) and 1% penicillin/streptomycin (Gibco, 15140-122).
168 Cells were cultured at 37°C in a humidified incubator with a 5% CO_2 atmosphere. For experiments
169 with PMSCs, cells were cultured and their myogenic characteristics were verified as previously
170 described [36]. All animal procedures and experimental protocols were conducted in accordance
171 with the Declaration of Helsinki, and the protocol was approved by the Animal Ethics Committee
172 of the Faculty of Veterinary Science, Mahidol University (FVS-MU-IACUC: COA No. MUVS-
173 2023-07-40). Briefly, fresh semitendinosus muscles were harvested from 1-week-old Duroc
174 piglets. Subsequent experiments with porcine satellite cells were conducted between P3 and P6.
175 Dovitinib (MedChemExpress, HY-50905) and methylergometrine (Expogin®, 0460228) were the
176 test compounds. Their respective vehicle controls were dimethyl sulfoxide (DMSO) and
177 phosphate-buffered saline (PBS).

178 **2.5 Cell viability assay.** C2C12 myoblasts were seeded at a density of 2×10^3 cells per well in
179 96-well plates and cultured in growth medium (GM) for 24 h. Cells were then treated with
180 dovitinib (0.3125, 0.625, 1.25, 2.5, and 5 μM) or methylergometrine (1.25, 2.5, 5, 10, and 20 μM)



181 for 24 or 48 h. Cell viability was evaluated using MTT assay. Briefly, cells were incubated with
182 0.5% MTT solution (3-(4,5-dimethylthiazol-2-yl)-2,5-diphenyltetrazolium bromide (Sigma-
183 Aldrich, M5655) for 2 h at 37 °C to allow the formation of insoluble formazan crystals. Following
184 incubation, the supernatant was carefully aspirated, and the formazan crystals were dissolved in
185 100% DMSO. Absorbance was measured at 570 nm using a Multiskan GO microplate
186 spectrophotometer (Thermo Scientific, USA).

187 **2.6 Myogenic differentiation assessment.** To evaluate the effects of the tested compounds on
188 myogenesis, C2C12 cells were used to assess early and late differentiation phases. Cells were
189 cultured in GM until reaching ~90% confluency and culture medium was replaced
190 with differentiation medium (DM), consisting of DMEM supplemented with 2% (v/v) horse serum
191 (HS; Gibco, 16050-130) and 1% penicillin/streptomycin at day 0. For early differentiation
192 assessment (Supplementary Fig. 1A), cells were plated at 7.5×10^3 cells/well and treated on
193 differentiation day 0. For late differentiation assessment (Supplementary Fig. 1B), cells were
194 plated at 1.2×10^5 cells/well with treatments administered on differentiation days 3-4. Cells were
195 treated with a range of concentrations of dovitinib (0 – 5 μ M) or methylergometrine (0 – 20 μ M).
196 For PMSCs, cells were cultured and treated to assess myogenic differentiation as follows. PMSCs
197 (passage 4) were plated at a density of 1×10^4 cells/well in iMatrix-coated 24-well plates and
198 cultured in DMEM supplemented with 20% FBS, 5 ng/ml basic fibroblast growth factor (bFGF),
199 and 20 μ M p38 inhibitor SB203580 (13067, Cayman Chemical, USA) and 1%
200 penicillin/streptomycin for 4 days (Supplementary Fig. 1C). After reaching ~90% confluency, the
201 culture medium was switched to DMEM supplemented with 2% HS to induce differentiation.



202 PMSCs were treated with dovitinib (0–1.25 μM) or methylergometrine (0–10 μM) on days 0, 2,
203 4, and 6 of the differentiation phases. Culture medium was replaced every other day.

204

205 **2.7 Immunofluorescence staining.** Cells were fixed with 4% paraformaldehyde (Sigma-Aldrich,
206 818715.0100) overnight at 4°C. Following fixation, cells were permeabilized with 0.1% Triton X-
207 100 (Scharlau, TR0447) and blocked with 5% normal goat serum (Invitrogen, PCN5000). The
208 primary antibody against myosin heavy chain (MHC) (Merck Millipore, 05-716) was incubated
209 for 2 h at room temperature. Subsequently, cells were incubated for 1 h with Alexa Fluor™ 594-
210 conjugated goat anti-mouse Ig cross-adsorbed secondary antibody (Invitrogen, A-11005) in the
211 dark. Nuclei were counterstained for 5 min with 4',6-diamidino-2-phenylindole (DAPI; Invitrogen,
212 D1306). Images were captured using an inverted fluorescence microscope (Olympus IX83)
213 equipped with an ORCA-Flash 2.8 digital CMOS camera (Hamamatsu Photonics, C11440).
214 Quantitative analysis was performed using OLYMPUS cellSens Dimension Desktop 4.3.1
215 software. The area fraction (%) of MHC-positive staining was measured as a key metric of
216 myogenic differentiation from 15 randomly captured images. The fusion index was calculated as
217 follows: the percentage of nuclei within multinucleated myotubes (defined as having ≥ 3 nuclei for
218 early differentiation or ≥ 10 nuclei for late differentiation) relative to the total number of nuclei in
219 the field. For the calculation of the differentiation index in PMSCs, all nuclei located within MHC-
220 positive myotubes were counted. Fusion and differentiation indices were acquired from the
221 randomization of 6 images.



222 **2.8 Western blot analysis.** Cellular protein was extracted using RIPA buffer (50 mM Tris-HCl
223 pH 7.5, 150 mM NaCl, 1 mM EDTA, 1% Triton X-100) supplemented with a protease inhibitor
224 cocktail (Sigma-Aldrich, P8340) and a phosphatase inhibitor cocktail (Merck Millipore, 524625).
225 Following centrifugation at $12,000 \times g$ for 15 min, the supernatant was collected, and protein
226 concentration was determined via a BCA assay (Thermo Scientific). Protein samples (10 μ g per
227 lane) were denatured and resolved on a SDS-polyacrylamide gel. The resolved proteins were then
228 transferred to a Nitrocellulose membrane (BIO-RAD, 1620112). Membranes were blocked with
229 5% nonfat milk and incubated overnight at 4°C with primary antibodies for myogenin
230 (MyoG) (1:200, Santa Cruz Biotechnology, SC-12732) and MHC (1:2,000, Merck Millipore, 05-
231 716). For loading control, a primary antibody against GAPDH (1:2,000, Cell Signaling
232 Technology, 2118) was used. Secondary horseradish peroxidase (HRP)-conjugated antibodies
233 (Cell Signaling Technology, anti-mouse 7076 and anti-rabbit 7074) were incubated for 1 h at room
234 temperature. Protein bands were visualized using a chemiluminescent HRP detection reagent
235 (Clarity™ Western ECL Substrate, BIO-RAD, 170-5060) and imaged with an Alliance Q9
236 Advanced Chemiluminescence Imager (UVITEC CAMBRIDGE). Quantification of protein
237 expression levels was performed using ImageJ software (version 1.54g, NIH).

238 **2.9 Statistical analysis.** Statistical significance was evaluated using GraphPad Prism version 10.
239 For comparisons involving multiple treatment groups against a single control, a one-way
240 ANOVA was performed, followed by Dunnett's multiple comparisons test. For direct pairwise
241 comparisons between two groups, an unpaired two-tailed Student's t-test with Welch's correction
242 was used, otherwise stated. A *p*-value of < 0.05 was considered statistically significant.



243
244
245
246
247
248
249
250
251
252
253
254
255
256
257
258
259
260

3. RESULTS AND DISCUSSION

3.1 *In silico* compound screening. To identify novel modulators of FGFR1 tyrosine kinase (FGFR1 TK), we initiated a comprehensive, multi-stage *in silico* screening campaign. Our primary goal was to find compounds that not only exhibit high binding affinity for FGFR1 but also possess favorable pharmacological properties and are economically viable for large-scale applications such as cultured meat production. The initial step involved a docking-based virtual screen of 872 pre-optimized ligands against the FGFR1 TK domain. Using dovitinib, a known FGFR1 inhibitor with a predicted binding energy (BE) of -8.8 kcal/mol, as a reference, we prioritized compounds with a BE of -8.8 kcal/mol or lower. This first round of screening yielded a substantial pool of 261 compounds with potentially high binding affinity to FGFR1 (Fig. 1A). To mitigate the risk of off-target effects, a crucial consideration for any therapeutic or biotechnological compound, we performed a secondary screening against p38 α mitogen-activated protein kinase (p38 α MAPK). This kinase is a pivotal regulator of terminal muscle cell differentiation [37]. Disruption of p38 α



261 MAPK signaling could counteract the desired myogenic effect, even if a compound effectively
262 inhibits FGFR1. Therefore, we sought compounds with a lower binding affinity (i.e., higher BE)
263 for p38 α MAPK. This counter-screening strategy, using the known p38 α MAPK inhibitor SCIO-
264 469 (BE = -10.4 kcal/mol) as a benchmark, successfully filtered out compounds with potential off-
265 target binding. This refined approach ultimately narrowed our selection to 20 promising candidates
266 (15 nuclear receptor compounds and 5 in-house compounds) that showed both strong FGFR1
267 binding and minimal predicted p38 α MAPK interaction (BE range: -6.0 to -9.3 kcal/mol; Fig. 1B).

268 Beyond molecular affinity, practical criteria for a functional compound
269 include solubility and cost. Poor solubility can severely limit a compound's bioavailability and
270 efficacy [38-40]. We therefore used the SwissADME web server to predict the solubility of the 20
271 shortlisted compounds via three distinct models: ESOL, Ali, and SILICOS-IT [41]. A compound
272 was considered "soluble" if at least two of the three models concurred, a stringent criterion that
273 further reduced our candidate pool to five compounds: nr848, nr796, nr101, nr12, and inh-1 (Fig.
274 1C). Finally, we evaluated the cost-effectiveness of these five candidates, a critical factor for the
275 commercial viability of cultured meat. Sourcing pricing information from publicly available
276 databases and, in the case of methylergometrine (inh-1), we found that methylergometrine was by
277 far the most affordable option. This multi-criteria analysis, which considered FGFR1 binding
278 affinity, off-target binding, solubility, and cost, led to the selection of methylergometrine as our
279 primary hit compound. Its 2D chemical structure is depicted in Fig. 1D, and its suitability for
280 further investigation was strongly supported by our comprehensive screening funnel.

281 **3.2 Structural dynamics and binding recognition.** To gain deeper insight into the binding
282 mechanism of our selected compounds, we conducted MD simulations of dovitinib and
283 methylergometrine in complex with FGFR1 TK. We first assessed the stability of the protein-
284 ligand complexes by analyzing the root-mean-square deviation (RMSD) of the protein backbone.
285 As shown in Fig. 2A, the RMSD profiles for both complexes indicated a stable system, with
286 fluctuations primarily originating from distal, flexible regions of the protein rather than the core
287 binding site. The methylergometrine-FGFR1 complex showed remarkable stability with less
288 fluctuation compared to the dovitinib complex, suggesting that methylergometrine forms a robust
289 and stable complex in a dynamic, aqueous environment. To identify the key amino acids involved
290 in binding, we performed a per-residue free energy decomposition analysis on the stable
291 trajectories (180–200 ns). We defined "hotspot" residues as those with a binding free energy
292 decomposition ($\Delta G_{bind}^{residue}$) of < -1.00 kcal/mol. This analysis revealed distinct yet overlapping
293 binding patterns. For dovitinib, key residues included Leu484, Val492, Glu562, Tyr563, Ala564,
294 Lys566, Gly567, and Leu630 (Fig. 2B-left). Methylergometrine, on the other hand, interacted with
295 Leu484, Val492, Ala512, Lys514, Met535, Ile545, Val561, Leu630, and Ala640 (Fig. 2B-right).
296 Intriguingly, both compounds shared interactions with Leu484, Val492, and Leu630, suggesting
297 they occupy a similar binding pocket within the FGFR1 active site. These residues have been
298 previously identified as crucial for the binding of other FGFR1 TK inhibitors like AZD4547 and
299 TKI258 [23, 42, 43], highlighting a shared mechanism of inhibition. Methylergometrine's
300 particularly strong interaction with Val492 and Leu630 further underscores its potential as a potent
301 FGFR1 modulator. The visualization of non-covalent interactions from the final MD snapshots



(Fig. 2C) confirmed that hydrophobic interactions were the dominant force driving the binding of both compounds. Dovitinib formed hydrophobic bonds with Leu484, Val492, Ala512, Ile545, Leu630, and Met535, while methylergometrine interacted hydrophobically with Ala512, Ala564, Leu630, and Val492. These findings are consistent with the negative van der Waals energy values observed in the MM/GBSA analysis (Table 1), indicating the critical role of these interactions in stabilizing the protein-ligand complexes.

3.3 End-point binding free energy. To quantitatively compare the binding affinities of dovitinib and methylergometrine, we used the end-point MM/GBSA method on the final 20 ns of the MD trajectories. As detailed in Table 1, both compounds exhibited strong, comparable binding affinities, with binding free energy (ΔG_{bind}) values of -21.84 ± 8.06 kcal/mol for dovitinib and -23.05 ± 6.86 kcal/mol for methylergometrine. The energy decomposition revealed that for both compounds, the binding was primarily driven by the favorable van der Waals interactions (ΔE_{vdw}) in the gas phase. The electrostatic contribution ($\Delta E_{electrostatic}$) was also favorable but approximately half the magnitude of the van der Waals term, reinforcing the dominance of hydrophobic forces. Interestingly, methylergometrine showed a more favorable solvation energy (ΔG_{solv}) but also a higher entropic penalty, indicating that while it fits well into the binding pocket, its binding is associated with a greater loss of conformational freedom. Overall, these results from MD simulations are highly consistent with the molecular docking predictions and provide strong theoretical support for the experimental validation.



321 **3.4 Experimental validation with STD-NMR Spectroscopy.** To provide direct experimental
322 evidence of the compound-protein interactions, we performed STD-NMR spectroscopy.
323 For dovitinib, the STD-NMR spectrum showed a clear signal at a single proton position (position
324 1, Fig. 3A), confirming a direct interaction with the recombinant FGFR1 protein. However, this
325 finding was discordant with our MD simulations, which did not predict this specific proton to be
326 in close proximity to the protein. This discrepancy likely stems from the inherent differences
327 between static computational models and the dynamic, in-solution environment of NMR. The high
328 RMSD fluctuations observed in the dovitinib complex during MD simulations also point to a
329 highly flexible binding mode or potential for multiple transient binding conformations, which
330 could explain the difference between the computational and experimental results. In contrast, the
331 STD-NMR results for methylegometrine were highly consistent with our MD simulations. A
332 strong STD signal was detected at proton position 1 (Fig. 3B), which the MD simulation predicted
333 to be in close contact with the key residue Val492. Weaker, but still detectable, STD signals were
334 also observed at positions 2, 3, and 4. Position 2 was computationally placed near Val492, while
335 positions 3 and 4 were near Asp641, a residue that formed a hydrogen bond with the ligand's
336 neighboring oxygen. The convergence of these experimental and computational findings provides
337 compelling evidence that methylegometrine directly and specifically binds to FGFR1 through
338 multiple contact points, making it a robust candidate for modulating its activity.

339 **3.5 Enhancing C2C12 differentiation with dovitinib and methylegometrine.** To establish a
340 robust *in vitro* screening framework, we employed the immortalized C2C12 murine cell line [44],
341 a strategy underpinned by the high evolutionary conservation of the FGFR1 tyrosine kinase



342 domain across human, mouse, and porcine species (Supplementary Fig. 2). Preliminary safety
343 profiling revealed distinct cytotoxic signatures for each candidate. While methylergometrine
344 demonstrated high biocompatibility with IC_{50} values consistently exceeding 20 μ M at both 24 and
345 48 h, dovitinib exhibited a time-dependent cytotoxic profile, with the IC_{50} shifting from >5 μ M at
346 24 h to 2.1 μ M at 48 h. These pharmacological thresholds informed the selection of sub-toxic
347 concentrations for subsequent functional assays, wherein the pro-myogenic efficacy of both
348 dovitinib and methylergometrine was evaluated across the discrete early and late phases of
349 myogenic differentiation.

350 In the subsequent experiment, the effects of dovitinib and methylergometrine were assessed on
351 C2C12 myogenic differentiation during both early and late myogenic differentiation phases. At
352 low concentrations (0.3125-0.625 μ M), dovitinib significantly enhanced the expression of MHC,
353 a key marker of myotube formation, in the early phase (Fig. 4A-B). This effect was most
354 pronounced at 0.625 μ M, where MHC expression was $\sim 123\%$ of the control ($p < 0.001$).
355 Interestingly, higher concentrations were detrimental, reducing myotube formation. In the late
356 phase, a dose-dependent increase in myotube size was observed (Fig. 4A), and quantitative
357 analysis confirmed a significant increase in MHC expression from 1.25 to 5 μ M (Fig. 4C).
358 The fusion index, a measure of myoblast fusion into multinucleated myotubes [45, 46]. A slight,
359 non-significant increase was observed at 0.625 μ M during the early phase (Fig. 4D), whereas a
360 significant increase was detected in the late phase at 2.5 μ M ($\sim 134\%$ of control, $p < 0.05$) (Fig.
361 4E), suggesting that dovitinib primarily promotes myotube maturation and fusion rather than the
362 initial commitment to differentiation. Next, we investigated methylergometrine's effects. In the



363 early phase, methylergometrine significantly enhanced MHC expression at 5 μM (~140% of
364 control, Fig. 5A-B), with a notable increase in myotube size and length. In the late phase, MHC
365 expression showed a gradual, dose-dependent increase from 2.5 to 20 μM (Fig. 5C), with peak
366 effects at 20 μM . The fusion index in the early phase at 5 μM (~150% of control, Fig. 5D) was also
367 significantly increased, indicating a potent ability to drive early fusion events, whereas no
368 significant change was observed in the late phase at 10 μM (Fig. 5E). These immunofluorescence
369 results suggest a phase-specific effect for each compound. Dovitinib appears to be most effective
370 during the later stages of myogenesis, promoting myotube maturation, while methylergometrine
371 is a powerful driver of early myoblast fusion.

372 In this study, serum-containing medium was utilized as it provides a complex physiological
373 background rich in pro-proliferative growth factors, which naturally suppress the onset of
374 myogenesis. By demonstrating that dovitinib and methylergometrine can effectively trigger
375 terminal differentiation even within this mitogen-heavy environment, we provide a robust proof-
376 of-concept for their ability to physiologically override endogenous proliferative signals.
377 Furthermore, utilizing serum-containing medium baseline minimizes potential confounding
378 variables—such as non-specific cellular stress or metabolic stagnation—that are frequently
379 associated with unoptimized serum-free formulations. This ensures that the accelerated myotube
380 formation observed is a direct result of targeted FGFR1 modulation rather than a secondary
381 response to nutrient deprivation.



382 **3.6 Dovitinib and methylergometrine increase MHC and MyoG expression during myogenic**
383 **differentiation.** To corroborate our immunofluorescence findings, we performed Western blot
384 analysis to quantify the expression levels of key myogenic markers: MyoG (a master regulator of
385 myogenic differentiation) and MHC. Consistent with our imaging data, both dovitinib and
386 methylergometrine significantly upregulated MyoG and MHC expression in a dose- and phase-
387 dependent manner. For dovitinib, early-phase treatment at 0.625 μM led to a dramatic ~ 4.5 -fold
388 increase in MHC expression and a ~ 3.4 -fold increase in MyoG at 0.3125 μM (Fig. 6A, C). In the
389 late phase, both markers showed robust, dose-dependent increases (Fig. 6B, D), further supporting
390 dovitinib's role in promoting myotube maturation. Similarly, methylergometrine significantly
391 upregulated MyoG and MHC expression. In the early phase, MHC peaked at 5 μM (~ 2.6 -fold
392 increase) and MyoG at 1.25 μM (~ 2.2 -fold increase) (Fig. 6E, G). Late-phase treatment also
393 resulted in a significant and dose-dependent increase for both markers (Fig. 6F, H). Collectively,
394 these results from both imaging and Western blot analyses paint a clear picture: dovitinib and
395 methylergometrine are potent enhancer of myogenic differentiation, but they appear to act with
396 slightly different temporal profiles. Dovitinib seems to be a more effective molecular switch for
397 priming differentiation and driving terminal maturation, while methylergometrine shows a strong
398 capacity for enhancing myoblast fusion and morphological development, particularly in the early
399 phase. Beyond the induction of well-known myogenic markers, efficient myogenic differentiation
400 for cultured meat applications requires coordinated regulation of cellular metabolism to sustain
401 high levels of protein synthesis and tissue maturation. FGFR1 signaling has been reported to
402 intersect with the PI3K–AKT–mTOR axis, a pathway that promotes cellular growth [47].



403 Therefore, the observed upregulation of MyoG and MHC in this study may reflect enhanced
404 myogenic lineage commitment and an increased capacity for muscle-specific protein synthesis,
405 which is essential for generating sufficient biomass and maintaining structural integrity in a
406 cultured meat system. Myogenic differentiation may also be accompanied by metabolic
407 remodeling, including increased mitochondrial biogenesis and a shift toward oxidative
408 metabolism, to meet the elevated energy demands associated with myotube formation and
409 maturation [48, 49]. Modulation of FGFR1 signaling may thus indirectly support mitochondrial
410 function, ensuring adequate ATP supply during differentiation. In parallel, coordinated regulation
411 of lipid and fatty acid metabolism has been reported during myogenesis, contributing to membrane
412 expansion, energy homeostasis, and the development of muscle tissue architecture [50]. Although
413 mitochondrial activity and lipid metabolism were not directly assessed in the present study, these
414 processes represent important downstream consequences of FGFR1 modulation and are
415 particularly relevant in the context of cultured meat production, where both differentiation
416 efficiency and metabolic robustness critically influence yield, consistency, and product quality.

417 **3.7 Translational validation in porcine muscle stem cells (PMSCs).** To evaluate the
418 translational viability of our findings for cellular agriculture, we validated the pro-myogenic
419 efficacy of dovitinib and methylergometrine in PMSCs. Immunofluorescence analysis of MHC
420 expression revealed divergent pharmacological profiles for the two compounds (Fig. 7A–B).
421 Dovitinib exhibited a narrow, biphasic therapeutic window; while a low concentration (0.3125
422 μM) significantly enhanced the differentiation index (Fig. 7C), a dose of 1.25 μM proved
423 cytotoxic, markedly suppressing both MHC expression and total cell viability. In sharp contrast,



424 methylergometrine demonstrated a robust, dose-dependent promotive effect on myotube
425 formation, with 5 μM significantly increasing the differentiation index relative to controls (Fig.
426 7D). This was further corroborated by linear regression analysis, which identified a significant
427 positive dose–response relationship for methylergometrine ($p=0.017$), a correlation notably absent
428 for dovitinib due to its inhibitory effects at higher concentrations. These species-specific results
429 underscore the necessity of validating hits from immortalized models in primary target cells. Given
430 their distinct kinetic profiles, we propose a strategic, sequential application: low-dose dovitinib
431 may serve as an initial molecular trigger for the myogenic program, while methylergometrine
432 drives sustained cellular fusion and structural maturation, providing a dual-action framework for
433 optimizing high-quality muscle tissue formation in cultured meat production.

434 4. CONCLUSION

435 This study identifies and characterizes dovitinib and methylergometrine as potent modulators of
436 myogenic differentiation through FGFR1 inhibition. Targeted modulation of FGFR1 signaling
437 enhances myogenic progression by upregulating key differentiation makers, MyoG and MHC, and
438 promoting myotube formation in both C2C12 and PMSCs. This phenomenon can support cellular
439 programs that are essential for muscle tissue formation, including increased protein synthesis
440 capacity and metabolic adaptation during myogenesis. Notably, the phase-dependent effects
441 observed for dovitinib and methylergometrine suggest a potential dual-phase differentiation
442 strategy, in which early and late fusion events of myotube formation can be selectively enhanced.
443 Dovitinib serves as the gold-standard inhibitor to prove the mechanism. Methylergometrine, while
444 a pharmaceutical, provides a scaffold for a more affordable, stable, and generally recognized as



445 safe derivative search. These are lead compounds meant to pave the way for identifying natural,
446 food-grade FGFR1 antagonists such as phytochemicals with similar binding motifs. This concept
447 is particularly relevant to cultured meat production, where efficient differentiation and metabolic
448 stability are critical determinants of tissue quality and production consistency. As FGFR1
449 modulation likely influences the metabolic partitioning of nutrients into protein versus
450 intramyocellular lipids, future studies may include a full lipidomic profile or total crude protein
451 analysis. Together, these findings support FGFR1 modulation by small molecules as a practical
452 approach to improving muscle tissue formation in scalable cultured meat systems.

453 REFERENCES

- 454 1. Wu, G., *Dietary protein intake and human health*. Food Funct, 2016. **7**: p. 1251-1265.
- 455 2. Bauer, J., et al., *Evidence-based recommendations for optimal dietary protein intake in*
456 *older people: a position paper from the PROT-AGE Study Group*. J Am Med Dir Assoc,
457 2013. **14**(8): p. 542-59.
- 458 3. Post, M.J., *Cultured meat from stem cells: Challenges and prospects*. Meat Science,
459 2012. **92**(3): p. 297-301.
- 460 4. Bryant, C. and J. Barnett, *Consumer acceptance of cultured meat: A systematic review*.
461 Meat Science, 2018. **143**: p. 8-17.
- 462 5. Blanton, J.R., Jr., et al., *Isolation of two populations of myoblasts from porcine skeletal*
463 *muscle*. Muscle Nerve, 1999. **22**(1): p. 43-50.
- 464 6. Wilschut, K.J., et al., *Isolation and characterization of porcine adult muscle-derived*
465 *progenitor cells*. J Cell Biochem, 2008. **105**(5): p. 1228-39.



- 466 7. Kadim, I.T., et al., *Cultured meat from muscle stem cells: A review of challenges and*
467 *prospects*. Journal of Integrative Agriculture, 2015. **14**(2): p. 222-233.
- 468 8. Guan, X.Y., Q.; Ma, Z.; Zhou, J., *Production of mature myotubes in vitro improves the*
469 *texture and protein quality of cultured pork*. Food Funct, 2023. **14**: p. 3576-3587.
- 470 9. Ma, T., et al., *Transdifferentiation of fibroblasts into muscle cells to constitute cultured*
471 *meat with tunable intramuscular fat deposition*. Elife, 2024. **13**.
- 472 10. Melzener, L., et al., *Optimisation of cell fate determination for cultured muscle*
473 *differentiation*. bioRxiv, 2023: p. 2023.09.06.556523.
- 474 11. Dombrowski, C., et al., *FGFR1 signaling stimulates proliferation of human mesenchymal*
475 *stem cells by inhibiting the cyclin-dependent kinase inhibitors p21(Waf1) and p27(Kip1)*.
476 Stem Cells, 2013. **31**(12): p. 2724-36.
- 477 12. Feng, Y., et al., *A feedback circuit between miR-133 and the ERK1/2 pathway involving*
478 *an exquisite mechanism for regulating myoblast proliferation and differentiation*. Cell
479 Death Dis, 2013. **4**(11): p. e934.
- 480 13. Zhan, S., et al., *LncR-133a Suppresses Myoblast Differentiation by Sponging miR-133a-*
481 *3p to Activate the FGFR1/ERK1/2 Signaling Pathway in Goats*. Genes (Basel), 2022.
482 **13**(5).
- 483 14. Li, H.K., et al., *LRTM1 promotes the differentiation of myoblast cells by negatively*
484 *regulating the FGFR1 signaling pathway*. Exp Cell Res, 2020. **396**(1): p. 112237.
- 485 15. Liang, D., et al., *Insight into resistance mechanisms of AZD4547 and E3810 to FGFR1*
486 *gatekeeper mutation via theoretical study*. Drug Des Devel Ther, 2017. **11**: p. 451-461.



- 487 16. Perdios, L., et al., *Conformational transition of FGFR kinase activation revealed by site-*
488 *specific unnatural amino acid reporter and single molecule FRET*. Sci Rep, 2017. **7**: p.
489 39841.
- 490 17. Mahapatra, S., et al., *Molecular dynamics simulations reveal phosphorylation-induced*
491 *conformational dynamics of the fibroblast growth factor receptor 1 kinase*. J Biomol
492 Struct Dyn, 2024. **42**(6): p. 2929-2941.
- 493 18. Cala, O., F. Guillièrè, and I. Krimm, *NMR-based analysis of protein-ligand interactions*.
494 Anal Bioanal Chem, 2014. **406**(4): p. 943-56.
- 495 19. Mayer, M. and B. Meyer, *Characterization of Ligand Binding by Saturation Transfer*
496 *Difference NMR Spectroscopy*. Angew Chem Int Ed Engl, 1999. **38**(12): p. 1784-1788.
- 497 20. André, F., et al., *Targeting FGFR with dovitinib (TKI258): preclinical and clinical data*
498 *in breast cancer*. Clin Cancer Res, 2013. **19**(13): p. 3693-702.
- 499 21. Lee, Y., et al., *A Receptor Tyrosine Kinase Inhibitor, Dovitinib (TKI-258), Enhances*
500 *BMP-2-Induced Osteoblast Differentiation In Vitro*. Mol Cells, 2016. **39**(5): p. 389-94.
- 501 22. Bateman, B.T., et al., *Methylergonovine maleate and the risk of myocardial ischemia and*
502 *infarction*. Am J Obstet Gynecol, 2013. **209**(5): p. 459.e1-459.e13.
- 503 23. Tucker, J.A., et al., *Structural insights into FGFR kinase isoform selectivity: diverse*
504 *binding modes of AZD4547 and ponatinib in complex with FGFR1 and FGFR4*.
505 Structure, 2014. **22**(12): p. 1764-1774.
- 506 24. Azevedo, R., et al., *X-ray structure of p38 α bound to TAK-715: comparison with three*
507 *classic inhibitors*. Acta Crystallogr D Biol Crystallogr, 2012. **68**(Pt 8): p. 1041-50.
- 508 25. O'Boyle, N.M., et al., *Open Babel: An open chemical toolbox*. J Cheminform, 2011. **3**: p.
509 33.



- 510 26. Koebel, M.R., et al., *AutoDock VinaXB: implementation of XBSF, new empirical halogen*
511 *bond scoring function, into AutoDock Vina*. J Cheminform, 2016. **8**: p. 27.
- 512 27. Jurrus, E., et al., *Improvements to the APBS biomolecular solvation software suite*.
513 Protein Sci, 2018. **27**(1): p. 112-128.
- 514 28. Tian, C., et al., *ff19SB: Amino-Acid-Specific Protein Backbone Parameters Trained*
515 *against Quantum Mechanics Energy Surfaces in Solution*. J Chem Theory Comput, 2020.
516 **16**(1): p. 528-552.
- 517 29. Darden, T.Y., D.; Pedersen, L., *Particle Mesh Ewald: An $N\text{-log}(N)$ Method for Ewald*
518 *Sums in Large Systems*. The Journal of Chemical Physics, 1993. **98**: p. 10089-10092.
- 519 30. Berendsen, H.J.C.P., J. P. M. ; van Gunsteren, W. F. ; DiNola, A. ; Haak, J. R.,
520 *Molecular dynamics with coupling to an external bath*. . The Journal of Chemical
521 Physics, 1984. **81**(8): p. 3684-3690.
- 522 31. Uberuaga, B.P., M. Anghel, and A.F. Voter, *Synchronization of trajectories in canonical*
523 *molecular-dynamics simulations: observation, explanation, and exploitation*. J Chem
524 Phys, 2004. **120**(14): p. 6363-74.
- 525 32. Paterlini, M.G. and D.M. Ferguson, *Constant temperature simulations using the Langevin*
526 *equation with velocity Verlet integration*. Chemical Physics, 1998. **236**(1): p. 243-252.
- 527 33. Ryckaert, J.-P., G. Ciccotti, and H.J.C. Berendsen, *Numerical integration of the cartesian*
528 *equations of motion of a system with constraints: molecular dynamics of n-alkanes*.
529 Journal of Computational Physics, 1977. **23**(3): p. 327-341.
- 530 34. Roe, D.R. and T.E. Cheatham, 3rd, *PTRAJ and CPPTRAJ: Software for Processing and*
531 *Analysis of Molecular Dynamics Trajectory Data*. J Chem Theory Comput, 2013. **9**(7): p.
532 3084-95.



- 533 35. Miller, B.R., 3rd, et al., *MMPBSA.py: An Efficient Program for End-State Free Energy*
534 *Calculations*. J Chem Theory Comput, 2012. **8**(9): p. 3314-21.
- 535 36. Suriya, U., et al., *A diarylheptanoid derivative mediates glycogen synthase kinase 3 β to*
536 *promote the porcine muscle satellite cell proliferation: Implications for cultured meat*
537 *production*. Biochem Biophys Res Commun, 2024. **736**: p. 150850.
- 538 37. Cabane, C., et al., *Regulation of C2C12 myogenic terminal differentiation by*
539 *MKK3/p38alpha pathway*. Am J Physiol Cell Physiol, 2003. **284**(3): p. C658-66.
- 540 38. Di, L., P.V. Fish, and T. Mano, *Bridging solubility between drug discovery and*
541 *development*. Drug Discov Today, 2012. **17**(9-10): p. 486-95.
- 542 39. Alsenz, J. and M. Kansy, *High throughput solubility measurement in drug discovery and*
543 *development*. Advanced Drug Delivery Reviews, 2007. **59**(7): p. 546-567.
- 544 40. Kennedy, T., *Managing the drug discovery/development interface*. Drug Discovery
545 Today, 1997. **2**(10): p. 436-444.
- 546 41. Daina, A., O. Michielin, and V. Zoete, *SwissADME: a free web tool to evaluate*
547 *pharmacokinetics, drug-likeness and medicinal chemistry friendliness of small molecules*.
548 Sci Rep, 2017. **7**: p. 42717.
- 549 42. Leechaisit, R., et al., *Design, Synthesis, Biological Evaluation and Molecular Modeling*
550 *Studies of Novel Naphthoquinone-Triazole Hybrids as Potential FGFR1 Tyrosine Kinase*
551 *Inhibitors*. Asian Journal of Organic Chemistry, 2025. **14**(5): p. e202400813.
- 552 43. Bunney, T.D., et al., *The Effect of Mutations on Drug Sensitivity and Kinase Activity of*
553 *Fibroblast Growth Factor Receptors: A Combined Experimental and Theoretical Study*.
554 EBioMedicine, 2015. **2**(3): p. 194-204.



- 555 44. Sharples, A.P., et al., *Modelling in vivo skeletal muscle ageing in vitro using three-*
556 *dimensional bioengineered constructs*. Aging Cell, 2012. **11**(6): p. 986-95.
- 557 45. Terrie, L., et al., *Enhancing Myoblast Fusion and Myotube Diameter in Human 3D*
558 *Skeletal Muscle Constructs by Electromagnetic Stimulation*. Front Bioeng Biotechnol,
559 2022. **10**: p. 892287.
- 560 46. Noë, S., et al., *The Myotube Analyzer: how to assess myogenic features in muscle stem*
561 *cells*. Skelet Muscle, 2022. **12**(1): p. 12.
- 562 47. Zhang, D., et al., *FGFR1 Induces Acquired Resistance Against Gefitinib By Activating*
563 *AKT/mTOR Pathway In NSCLC*. Onco Targets Ther, 2019. **12**: p. 9809-9816.
- 564 48. Wagatsuma, A. and K. Sakuma, *Mitochondria as a potential regulator of myogenesis*.
565 ScientificWorldJournal, 2013. **2013**: p. 593267.
- 566 49. Sin, J., et al., *Mitophagy is required for mitochondrial biogenesis and myogenic*
567 *differentiation of C2C12 myoblasts*. Autophagy, 2016. **12**(2): p. 369-80.
- 568 50. Fabre, P., et al., *Bioactive lipid mediator class switching regulates myogenic cell*
569 *progression and muscle regeneration*. Nat Commun, 2025. **16**(1): p. 5578.

570

571

572

573

574

575



576

577

578

579

580

581

582 Author Contributions

583 All authors have full access to the data and accept responsibility for publication. SU, US, and TJ
584 have accessed and verified all data reported in this study. All authors have read, reviewed, and
585 agreed to the final manuscript. US and TJ conceptualised the study. RS, US, TJ designed the
586 experiments. SU, PC, SK, SW, WW, RS, TS, DL and US performed the investigation. SU, SK,
587 RS, US and TJ performed the formal analysis. SU, US, and TJ curated the data. TJ acquired
588 funding and did the project administration. SK, RS, DL, US and TJ provided resources. TJ
589 supervised the project. SU and US wrote the original draft. All authors reviewed and edited the
590 manuscript.

591 Funding Sources

592 This research project is supported by the NSRF via the Program Management Unit for Human
593 Resources & Institutional Development, Research and Innovation (B05F650014).

594 **Acknowledgment**

595 We acknowledge the Second Century Fund (C2F), Chulalongkorn University for a postdoctoral
596 fellowship to SU.

597 **Abbreviations**

598 PMSCs, porcine muscle stem cells; FGFR1, fibroblast growth factor receptor 1; MD, molecular
599 dynamics; NMR, nuclear magnetic resonance; STD, saturation transfer difference; DMEM,
600 Dulbecco's modified Eagle's medium; PBS, phosphate-buffered saline; DM, differentiation
601 medium; HRP, horseradish peroxidase; FGFR1 TK; FGFR1 tyrosine kinase; BE, binding energy;
602 MAPK, mitogen-activated protein kinase; RMSD; root-mean-square deviation.

603 **TABLE**

604 **Table 1: MM/GBSA energy components and binding free energy for FGFR1-ligand**
605 **complexes.** Values are in kcal/mol and represent means \pm S.D. from the final 20-ns MD
606 trajectories.

Energy components	Dovitinib	Methylergometrine
Gas phase (MM)		
$\Delta E_{\text{electrostatic}}$	-24.8905 ± 2.9841	-22.4979 ± 5.0582
ΔE_{vdW}	-41.2709 ± 3.7583	-46.4489 ± 3.0806
ΔE_{gas}	-66.1614 ± 5.5764	-68.9468 ± 4.9408
Solvation (GBSA)		



ΔG_{polar}	30.9189 ± 3.3940	26.4121 ± 3.8196
$\Delta G_{\text{nonpolar}}$	-4.5782 ± 0.2700	-6.0067 ± 0.1635
ΔG_{solv}	26.3407 ± 3.3494	20.4054 ± 3.8826
ΔH	-39.8207 ± 5.2667	-48.5414 ± 4.9783
$-T\Delta S$	17.9829 ± 6.1009	25.4924 ± 4.7232
$\Delta G_{\text{bind}} (MM/GBSA)$	-21.8378 ± 8.0597	-23.0490 ± 6.8624

607

608

609

610

611

612 **FIGURE LEGENDS**

613 **Figure 1: Hit compound identification via multi-criteria virtual screening.** (A) Scatter plot of
614 binding energies for 261 candidate compounds and dovitinib (No. 258) against FGFR1 TK (black
615 squares) and off-target p38 α MAPK (red circles). Asterisks denote compounds selected for the
616 next round. (B) Solubility predictions for the 20 selected compounds using three models from
617 SwissADME. Red, yellow, and blue indicate poor, moderate, and good solubility, respectively.
618 (C) Cost estimation for the five final candidates. The cost of methylethergometrine (inh-1) was
619 obtained from a hospital pharmacy. (D) 2D chemical structure of methylethergometrine.



620 **Figure 2: FGFR1-ligand complex stability and interaction analysis.** (A) RMSD plots of the protein
621 backbone for the full complex (black) and the binding site residues (red) over a 200-ns MD
622 simulation. (B) Per-residue free energy decomposition profiles and (C) 2D interaction diagrams
623 showing the specific non-covalent interactions at the binding site for dovitinib (left) and
624 methylergometrine (right).

625 **Figure 3: STD-NMR spectra of FGFR1 complexes.** (A) Dovitinib-FGFR1 and (B)
626 Methylergometrine-FGFR1. Green: STD difference spectra of slice 8 of 16 of the imaging STD
627 experiment. Red: STD-off resonance spectra of slice 8 of 16 of the imaging STD experiment. Blue:
628 1D NMR spectrum of the sample acquired with a 90° pulse, water suppression.

629 **Figure 4: Effects of dovitinib on C2C12 differentiation.** (A) Representative
630 immunofluorescence images of MHC (red) and nuclei (blue) after treatment with varying
631 concentrations of dovitinib (0.312-5 μM) during the early and late differentiation phases. Scale
632 bars = 200 μm . (B-C) Quantification of MHC expression levels (% of control) and (D-E) Fusion
633 index (% of control), following dovitinib treatment during the early and late phases, respectively.
634 Fusion index (% of control) was analyzed in the effective concentrations. Data are presented as
635 means \pm standard deviation (SD) of three independent experiments. Statistical significance is
636 indicated as follows: * $p < 0.05$; ** $p < 0.01$; *** $p < 0.001$; **** $p < 0.0001$ compared with control.

637 **Figure 5: Effects of methylergometrine on C2C12 differentiation.** (A) Representative
638 immunofluorescence images of MHC (red) and nuclei (blue) after treatment with varying
639 concentrations of methylergometrine (1.25-20 μM) during the early and late differentiation phases.
640 Scale bars = 200 μm . (B-C) Quantification of MHC expression levels (% of control) and (D-E)



641 Fusion index (% of control) following methylergometrine treatment during the early and late
642 phases, respectively. Fusion index (% of control) was analyzed at the effective concentration of
643 5 μ M in the early and 10 μ M in the late differentiation phases. Data are presented as means \pm
644 standard deviation (SD) of three independent experiments. Statistical significance is indicated as
645 follows: * $p < 0.05$; ** $p < 0.01$; *** $p < 0.001$; **** $p < 0.0001$ compared with control.

646 **Figure 6: Western blot analysis of myogenic markers.** Representative Western blot analysis of
647 MHC and MyoG expression during the early and late phases following treatment with dovitinib
648 and methylergometrine. (A, B) Western blot analysis of MHC and MyoG expression in C2C12
649 cells treated with dovitinib during the (A) early and (B) late differentiation phases. (E-F)
650 Expression of the MHC and MyoG in response to methylergometrine treatment during the (E)
651 early and (F) late differentiation phases. GAPDH served as a loading control. “C” denotes the
652 control group cultured in differentiation medium containing vehicle for each treatment. (C, D)
653 Quantification of dovitinib-treated samples. (G, H) Quantification of methylergometrine-treated
654 samples. Data are presented as means \pm standard deviation (SD) of three independent experiments.
655 Statistical significance is indicated as follows: * $p < 0.05$; ** $p < 0.01$; *** $p < 0.001$ compared
656 with control.

657 **Figure 7: Differential modulation of myogenic differentiation in PMSCs by dovitinib and**
658 **methylergometrine.** Representative immunofluorescence images of PMSCs following a 7-day
659 differentiation period in the presence of indicated concentrations of (A) dovitinib and (B)
660 methylergometrine. Cells were stained for myosin heavy chain (MHC, red), and nuclei were
661 counterstained with DAPI (blue). Scale bars = 100 μ m. (C and D) Quantitative analysis of the



662 differentiation index, calculated as the percentage of total nuclei located within MHC-positive
663 myotubes. Data are presented as the mean \pm SD. Statistical significance relative to the vehicle
664 control group was calculated using a one-tailed t-test: * $p < 0.05$; ** $p < 0.01$; *** $p < 0.001$.

665
666
667
668
669
670
671
672
673
674
675
676
677
678
679
680
681
682
683
684
685



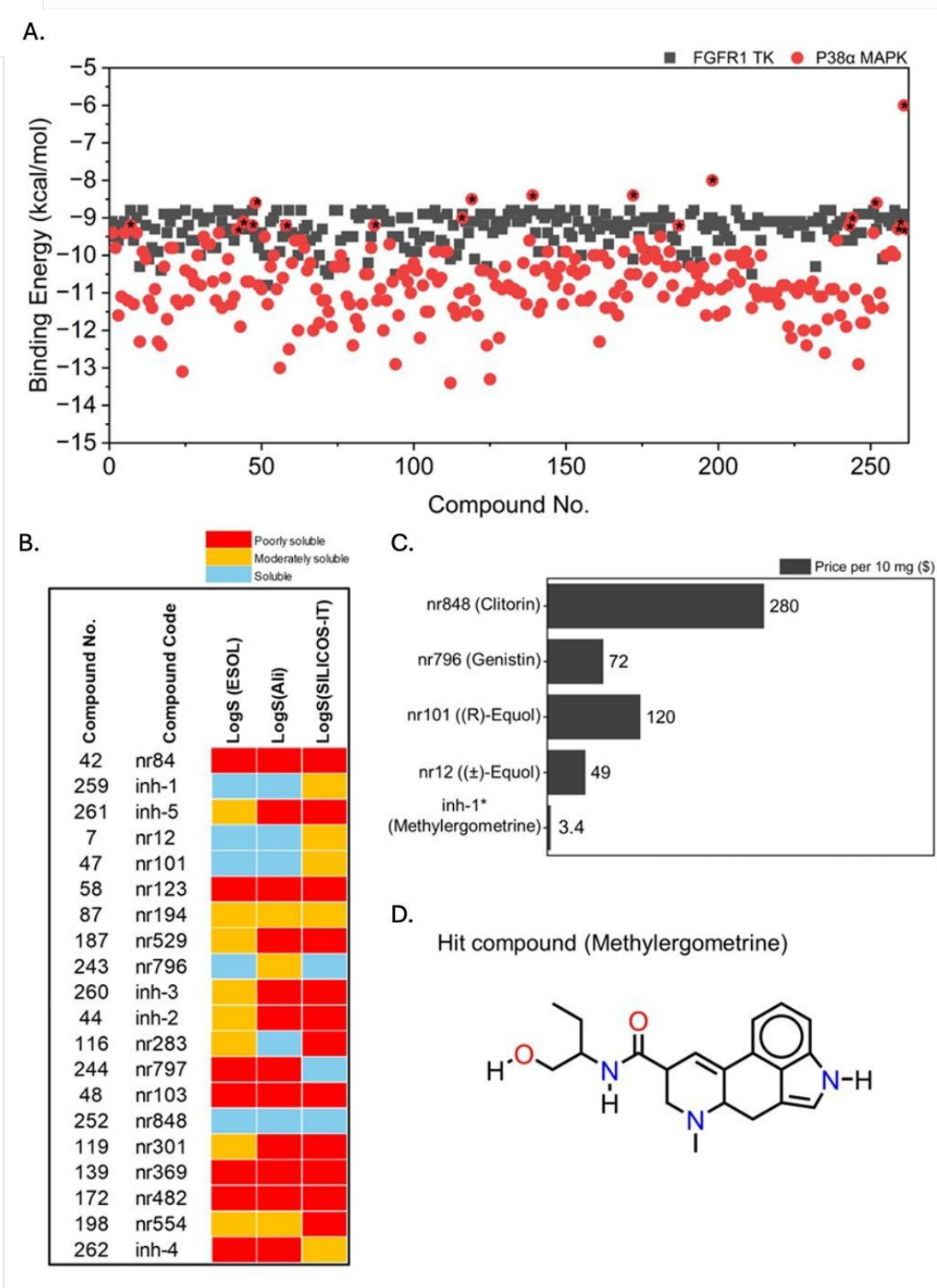
686
687
688
689
690
691
692
693
694
695
696
697
698
699
700
701
702
703
704
705
706

Open Access Article. Published on 11 March 2026. Downloaded on 3/12/2026 4:33:42 AM.
This article is licensed under a Creative Commons Attribution-NonCommercial 3.0 Unported Licence.



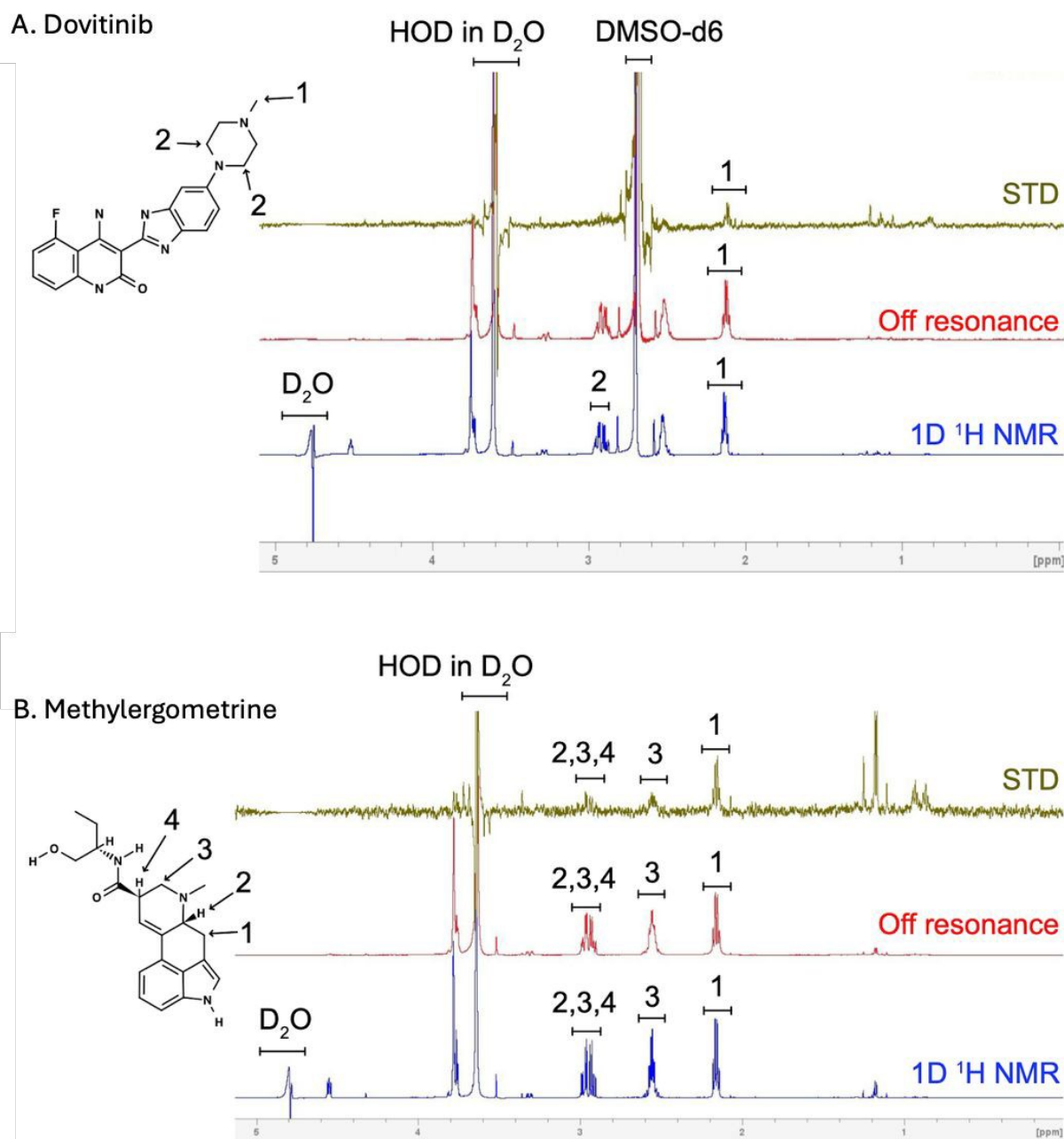
FIGURES

Figure 1



707

708 **Figure 2**



714

715

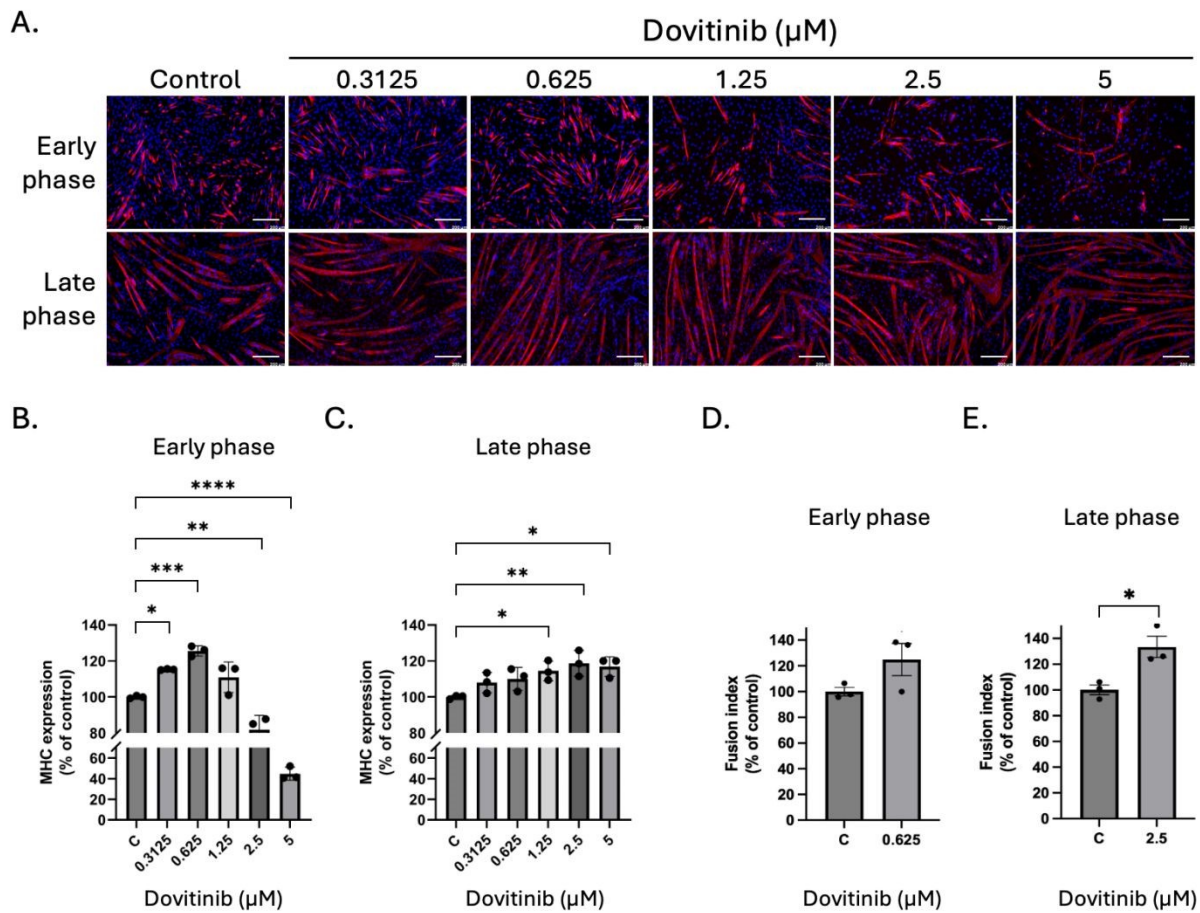
716

717

718

719

720 **Figure 4**



721

722

723

724

725

726

727

728

729

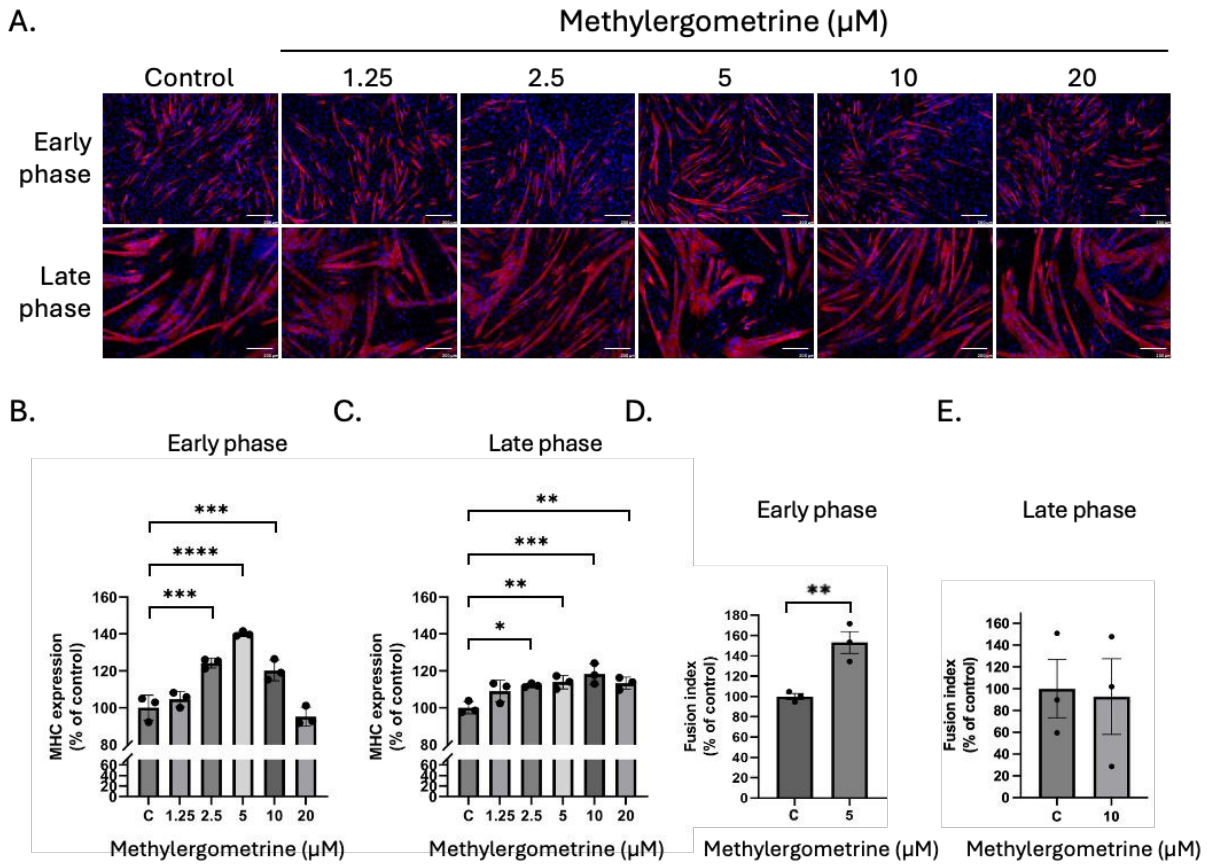
730

731

732

733

Figure 5



734

735

736

737

738

739

740

741

742

743

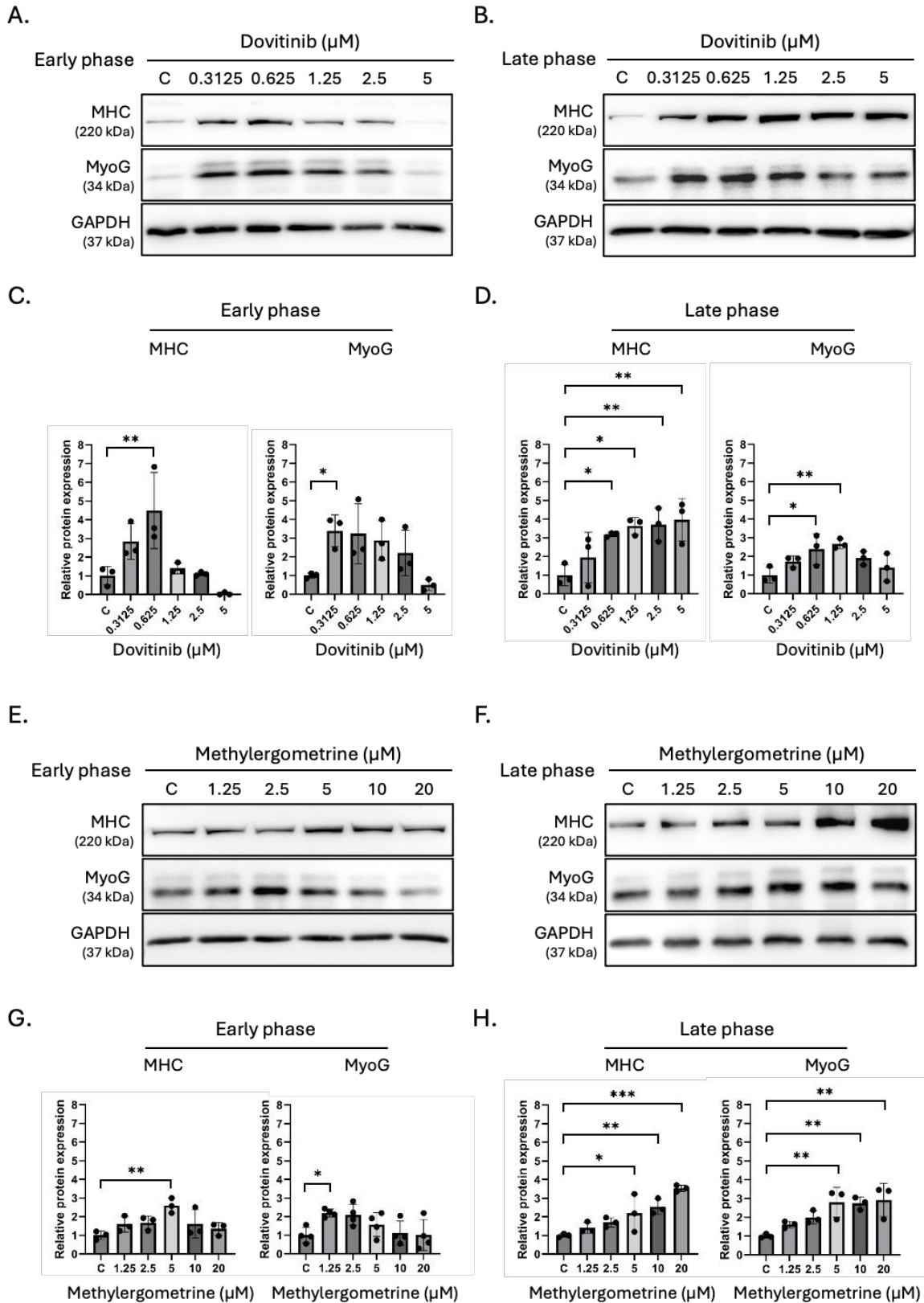
744

745

746

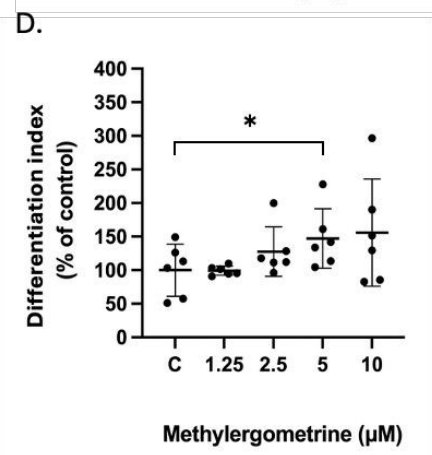
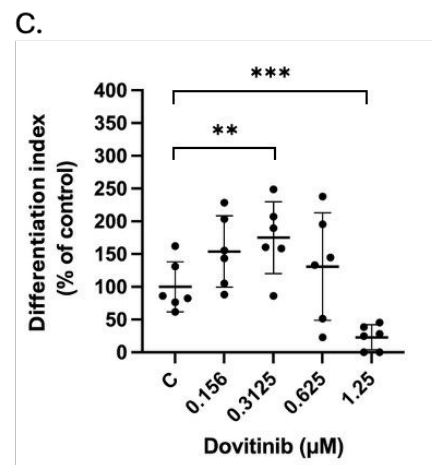
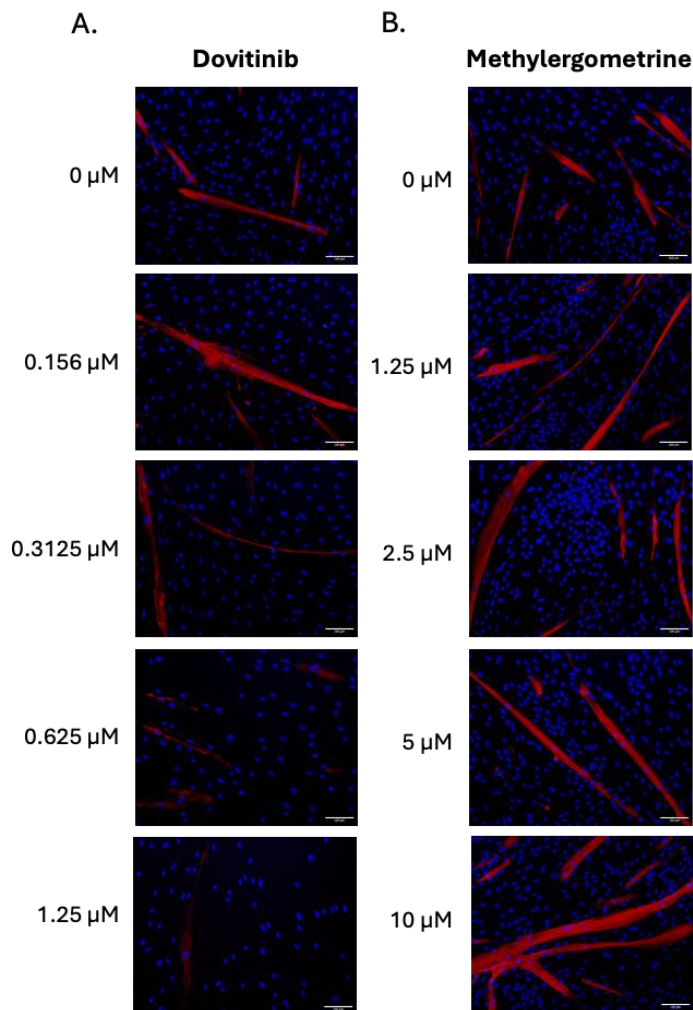
747

Figure 6



748

749 **Figure 7**



Open Access Article. Published on 11 March 2026. Downloaded on 3/12/2026 4:33:42 AM.
This article is licensed under a Creative Commons Attribution-NonCommercial 3.0 Unported Licence.



750
751
752
753
754
755
756
757
758
759
760

Data availability statements

The data supporting this article have been included as part of the Supplementary Information.

